Analysis of delocalization of clusters in linear-chain α -cluster states with entanglement entropy

Yoshiko Kanada-En'yo Department of Physics, Kyoto University, Kyoto 606-8502, Japan

I investigate entanglement entropy of one dimension (1D) cluster states to discuss the delocalization of clusters in linear-chain 3α - and 4α -cluster states. In analysis of entanglement entropy of 1D Tohsaki-Horiuchi-Schuck-Röpke (THSR) and Brink-Bloch cluster wave functions, I show clear differences in the entanglement entropy between localized cluster wave functions and delocalized cluster wave functions. In order to clarify spatial regions where the entanglement entropy is generated by the delocalization of clusters, I analyze the spatial distribution of entanglement entropy. In the linear-chain 3α cluster state, the delocalization occurs dominantly in a low-density tail region while it is relatively suppressed in an inner region because of Pauli blocking effect between clusters. In the linear-chain 4α state having a larger system size than the linear-chain 3α state, the delocalization occurs in the whole system. The entanglement entropy is found to be a measure of the delocalization of clusters in the 1D cluster systems.

I. INTRODUCTION

A variety of cluster states have been known in light nuclei, such as 2α states in 8 Be, 16 O + α states in 20 Ne, and 3α in 12 C (for example, see Ref. [1] and references therein). In this decade, a new concept of cluster states has been proposed to understand cluster motion in these states [2–7]. That is a dilute cluster gas state where clusters are not spatially localized in certain positions but they are rather freely moving like a gas. To describe the non-localized (delocalized) cluster states, a new type of cluster wave function, so-called "Tohsaki-Horiuchi-Schuck-Röpke" (THSR) wave function, has been introduced. The THSR wave function is essentially based on α clusters in a common Gaussian orbit having a range of the system size. It has been shown that the 2α state for $^8\text{Be}(0_1^+)$ and the 3α state for $^{12}\text{C}(0_2^+)$ can be well described by the THSR wave functions with a large Gaussian range compared with the cluster size, and therefore, these states are interpreted as gas-like cluster states of 2α and 3α . Recently, Zhou et al. have extended the THSR wave function to apply it to ^{20}Ne system, and shown that the THSR wave function can also describe the $^{16}\text{O}+\alpha$ states in ^{20}Ne [6, 7].

More recently, Suhara et al. have proposed that this concept of the α -cluster gas is applicable also to one dimension (1D) cluster motion in linear-chain $n\alpha$ structures [8]. Existence of the linear-chain $n\alpha$ states has been a long standing problem. In the early stage, Morinaga proposed a linear-chain 3α structure in $^{12}C(0_2^+)$ [9], but this assignment was excluded from the experimental data of its α decay width [10]. The possibility of the linear-chain 3α structure in a higher 0^+ state is now on discussion. Negative results for the linear-chain state were obtained by 3α -cluster models [1, 11], whereas appearance of a chain-like 3α state with an open triangle configuration was predicted by microscopic approaches with no cluster assumption and by an approach with the cluster breaking effect [12–15] and also by an ab initio calculation [16]. Also linear-chain 4α structures in ^{16}O have been attracting a great interest, and searching for linear-chain states have been performed in experimental and theoretical works in this line [17–22].

The conventional picture for the linear-chain $n\alpha$ structures is spatially localized α clusters arranged in 1D with certain intervals. Such a localized $n\alpha$ state is described by a single Brink-Bloch (BB) wave function [23]. The essential result shown by Suhara *et al.* is that the wave functions of the linear-chain 3α and 4α states are described by superposing a large number of BB wave functions, and surprisingly, they have large overlaps with 1D-THSR wave functions [8]. This result indicates that the delocalization occurs in 1D α -cluster motion and the linear-chain states can be regarded as 1D α cluster gases of delocalized clusters rather than localized cluster states. However, as shown in Ref. [8], the density distributions of the linear-chain states of 3α and 4α have three- and four-peak structures, respectively, which indicates partial localization of α clusters because of the Pauli blocking (repulsion) between α clusters. Even though the model in Ref. [8] was restricted in 1D configurations and the stability of the linear-chain states against bending motion and α decays have yet to be investigated for a conclusive answer to existence of the linear-chain states in realistic nuclear systems, their work provides the new picture of 1D cluster states, which is important to understand cluster phenomena in nuclear many-body systems, and also academically interesting.

In light nuclei, clusters are often formed by spatial correlations of constituent nucleons. Even in a mean-field picture, spatially correlated nucleons in a cluster can be described by a product of localized single-particle wave functions. However, such a localized cluster usually has much kinetic energy for the localization of center of mass motion (c.m.m.) of the cluster. If there is no potential nor Pauli blocking effect between clusters, it is naively expected that delocalization of the c.m.m. of clusters occurs to release the kinetic energy. An ideal case of the delocalization limit is a zero-momentum cluster gas state. The delocalization of clusters in realistic cluster states may depend on

competition between kinetic energy gain and energy loss by other effects such as potential and Pauli blocking between clusters.

To distinguish between localized and delocalized cluster structures in microscopic wave functions, one should carefully consider the antisymmetrization of nucleons between clusters, which strongly affects inter-cluster motion at a small distance. The antisymmetrization effect suppresses an amplitude of the inter-cluster wave function at a small inter-cluster distance and works as the Pauli repulsion (blocking) between clusters, whereas the effect vanishes at a large distance. If the system size is comparable to the cluster size, clusters can not move freely because of the Pauli blocking effect. Therefore, the delocalization of clusters likely occurs not in high-density regions but in low-density regions. Indeed, for two-body cluster states of 2α and $^{16}{\rm O} + \alpha$ in $^{8}{\rm Be}$ and $^{20}{\rm Ne}$, the author has shown that the delocalization of α clusters occurs at a long tail part of the inter-cluster motion [24]. Also in the result of the linear-chain 3α and 4α states shown by Suhara et al., the peak structure of density distributions shows the partial localization of α clusters in an inner region as mentioned previously. It may suggest the possibility that the delocalization does not occur in the whole region of the system. I should stress here that the THSR model wave functions, which can successfully describe cluster gas states, have characters of localization and/or delocalization of clusters depending on the system size relative to the cluster size. In the case that the system size is large enough compared with the cluster size, the THSR wave function actually describe a dilute cluster gas. However, if the system size is as small as the cluster size, the THSR wave function become equivalent to a localized cluster wave function because of the antisymmetrization. A general question is how one can understand the delocalization of clusters in an intermediate case between both limits of localization and delocalization. To clarify the region where the delocalization occurs, one may encounter a difficulty from the antisymmetrization, i.e., Pauli blocking effect. The Pauli blocking effect often makes it difficult to tell the difference between localization and delocalization of clusters in a relatively high-density region, where the delocalization is usually suppressed. Note that one can not obtain a definite answer from a wave function without the antisymmetrization, which may contain unphysical forbidden states.

My aim is to analyze the delocalization of clusters in microscopic wave functions with an approach free from the antisymmetrization effect. For this aim I propose a method of analysis using entanglement entropy defined by the one-body density matrix. The entanglement entropy has been introduced by Bennett et al. in 1996 [25], and widely used in various fields such as condensed matter and quantum field theory (see for example Refs. [26–28] and references therein). The entanglement entropy indicates how particles are entangled with other particles, and can be an indicator to measure many-body correlations as applied in in various fields such as condensed matter physics and quantum physics. For a system of independent Fermions, the wave function is given by a Slater determinant of single-particle wave functions, and the entanglement entropy completely vanishes. The entanglement entropy is generated by many-body correlations beyond a Slater determinant. In the case of cluster states, the entanglement entropy is zero in a single BB wave function for the localized cluster limit, and it is generated by the delocalization of clusters.

In this paper, I analyze the entanglement entropy in 1D cluster states for $n\alpha$ and $^{16}{\rm O} + \alpha$ systems. Based on the analysis of the entanglement entropy, I investigate the delocalization of clusters in the linear-chain 3α and 4α states predicted by Suhara *et al.* as well as the 2α state in $^8{\rm Be}(0^+_1)$ and the $^{16}{\rm O} + \alpha$ states in $^{20}{\rm Ne}(0^+_1)$ and $^{20}{\rm Ne}(1^-_1)$.

This paper is organized as follows. I describe the formulation in Section II. Section III discusses the entanglement entropy of 1D cluster states. The paper concludes with a summary in section IV.

II. FORMULATION

A. Wave functions for linear-chain $n\alpha$ -cluster structure

I consider the linear-chain $n\alpha$ -cluster structures aligned to the z axis (n is the number of α clusters). For simplicity, the angular momentum projection is not taken into account, and only 1D configurations of n α clusters in intrinsic wave functions are considered in the present analysis. It means that the (de)localization of α clusters are defined for α -cluster motion along the z axis. In this section, I first describe a general form of α -cluster wave functions for the linear-chain structures. More details of practical model wave functions used in the present paper are described in the latter part of this section.

1. BB wave function

I use the BB wave function [23] for a localized $n\alpha$ -cluster wave function,

$$\Phi_{\mathrm{BB}}^{n\alpha}(\mathbf{R}_{1},\ldots,\mathbf{R}_{n}) = \frac{1}{\sqrt{A!}} \mathcal{A} \left[\psi_{\mathbf{R}_{1}}^{\alpha} \cdots \psi_{\mathbf{R}_{n}}^{\alpha} \right], \tag{1}$$

$$\psi_{\mathbf{R}_{i}}^{\alpha} = \phi_{\mathbf{R}_{i}}^{0s} \chi_{p\uparrow} \phi_{\mathbf{R}_{i}}^{0s} \chi_{p\downarrow} \phi_{\mathbf{R}_{i}}^{0s} \chi_{n\uparrow} \phi_{\mathbf{R}_{i}}^{0s} \chi_{n\downarrow}, \tag{2}$$

$$\phi^{0s} = (\pi b^2)^{-3/4} \exp\left[-\frac{1}{2b^2}(\mathbf{r} - \mathbf{R}_i)^2\right].$$
 (3)

 $\psi_{\mathbf{R}_i}^{\alpha}$ is the four-nucleon wave function of the *i*th α cluster expressed by the $(0s)^4$ harmonic oscillator (ho) shell-model configuration localized around the spatial position \mathbf{R}_i . Note that a single BB wave function for an $n\alpha$ system is written by a Slater determinant of single-particle wave functions. For a linear-chain structure aligned to the z axis, the position parameter \mathbf{R}_i is set to be $\mathbf{R}_i = (0,0,R_i)$, and the 1D BB wave function is expressed as $\Phi_{\mathrm{BB}}^{n\alpha}(R_1,\ldots,R_n)$. The parameter b for the α -cluster size is chosen to be b=1.376 fm same as in Ref. [8]. General wave functions for 1D $n\alpha$ systems can be written by linear combination of BB wave functions $\Phi_{\mathrm{BB}}^{n\alpha}(R_1,\ldots,R_n)$.

2. 1D-THSR wave function

As shown in Ref. [8], the linear-chain 3α - and 4α -cluster states in 12 C and 16 O systems are well described by the 1D-THSR wave functions proposed by Suhara *et al.*. The 1D-THSR wave function is given by linear combination of BB wave functions with a Gaussian weight and it is in principle written as

$$\Phi_{\text{1D-THSR}}^{n\alpha}(\beta) = \int dR_1 \cdots dR_n \exp\left\{-\sum_{i=1}^n \frac{R_i^2}{\beta^2}\right\} \Phi_{\text{BB}}^{n\alpha}(R_1, \dots, R_n),$$

$$\propto \mathcal{A} \left[\prod_{i=1}^n \exp\left\{-\frac{2X_{ix}^2}{b^2} - \frac{2X_{iy}^2}{b^2} - \frac{X_{iz}^2}{\beta^2 + b^2/2}\right\} \phi(\alpha_i)\right],$$
(4)

where X_i is the center of mass (c.m.) coordinate of the ith α cluster and $\phi(\alpha_i)$ is the intrinsic wave function of the α cluster. If the antisymmetrization is ignored, the $\Phi_{\text{1D-THSR}}^{n\alpha}(\beta)$ expresses the $n\alpha$ state where all α clusters are confined in the x and y directions in the size $b/\sqrt{2}$ while they move in the z direction in the Gaussian orbit specified by the size parameter β , which corresponds to the system size of the linear-chain state. When β is large enough compared with the α -cluster size, the 1D-THSR wave function describes a dilute linear-chain gas where n α clusters move almost freely like a gas in the z direction. In the present calculation, the R_i integration is approximated by summation on mesh points in a finite box. The details are described later.

The BB and 1D-THSR wave functions contain the total c.m.m. In the present paper, the c.m.m. is not removed exactly because separation of the c.m. coordinate and intrinsic coordinates is technically difficult in calculation of the density matrix. In analysis of entropy in a system of 1α (one α) and that of an α cluster with a core, I keep the total c.m.m. as defined in the original form. For 2α , 3α , and 4α systems, I make a correction of the c.m.m. to eliminate a possible artifact from β dependence in the c.m.m. as explained later.

B. Entanglement entropy

I briefly describe entanglement entropy defined by the one-body density matrix. More detailed explanations are given in appendixes.

1. Density matrix

For a wave function $|\Psi^{(A)}\rangle$ for an A-nucleon state, the one-body density matrix $\rho^{(1)}$ is defined in the coordinate space as

$$\rho^{(1)}(\mathbf{r}\sigma;\mathbf{r}'\sigma') = \langle \Psi^{(A)} | a^{\dagger}(\mathbf{r}'\sigma')a(\mathbf{r}\sigma) | \Psi^{(A)} \rangle, \tag{5}$$

where $a^{\dagger}(r\sigma)$ and $a(r\sigma)$ are creation and annihilation operators of a nucleon at the position r with spin-isospin $\sigma = p \uparrow, p \downarrow, n \uparrow, n \downarrow$. The one-body density matrix is regarded as the matrix element of the density operator $\hat{\rho}_{\Psi}^{(1)}$ for the wave function $\Psi^{(A)}$,

$$\rho^{(1)}(\mathbf{r}\sigma;\mathbf{r}'\sigma') = \langle \mathbf{r}\sigma|\hat{\rho}_{\Psi}^{(1)}|\mathbf{r}'\sigma'\rangle. \tag{6}$$

The diagonal element of the density matrix $\rho^{(1)}(\mathbf{r}\sigma) = \rho^{(1)}(\mathbf{r}\sigma;\mathbf{r}\sigma)$ indicates the one-body density of σ nucleons at \mathbf{r} . Using the orthonormal single-particle bases $\{|l\rangle\}$ that diagonalize the density matrix, the density operator and density matrix are written as

$$\hat{\rho}_{\Psi}^{(1)} = \sum_{l} |l\rangle \rho_{l}^{(1)} \langle l|, \tag{7}$$

$$\rho^{(1)}(\boldsymbol{r}\boldsymbol{\sigma};\boldsymbol{r}'\boldsymbol{\sigma}') = \sum_{l} \langle \boldsymbol{r}\boldsymbol{\sigma}|l\rangle \rho_{l}^{(1)}\langle l|\boldsymbol{r}'\boldsymbol{\sigma}'\rangle,$$

$$= \sum_{l} \phi_{l}(\boldsymbol{r}\boldsymbol{\sigma}) \rho_{l}^{(1)} \phi_{l}^{*}(\boldsymbol{r}'\boldsymbol{\sigma}'),$$
(8)

where $\phi_l(r\sigma) = \langle r\sigma | l \rangle$ is the wave function for the single-particle state $|l\rangle$, and

$$\rho_l^{(1)} = \langle \Psi^{(A)} | a_l^{\dagger} a_l | \Psi^{(A)} \rangle, \tag{9}$$

$$0 \le \rho_l^{(1)} \le 1,\tag{10}$$

is the eigen value of the density matrix and indicates the occupation probability of the single-particle state $|l\rangle$. The trace of the density matrix $\rho^{(1)}$ equals to the particle number as

$$A = \text{Tr}\rho^{(1)} = \sum_{l} \rho_{l}^{(1)} = \sum_{\sigma} \int \rho^{(1)}(r\sigma)dr$$
 (11)

$$\rho^{(1)}(\boldsymbol{r}\sigma) = \sum_{l} \rho_{l}^{(1)} \phi_{l}^{*}(\boldsymbol{r}\sigma) \phi_{l}(\boldsymbol{r}\sigma), \tag{12}$$

2. Entanglement entropy

The entanglement entropy is defined by the one-body density matrix as,

$$S^{(1)} = -\text{Tr}\rho^{(1)}\log\rho^{(1)} = -\sum_{l}\rho_{l}^{(1)}\log\rho_{l}^{(1)}.$$
(13)

The entanglement entropy is zero if a wave function $|\Psi^{(A)}\rangle$ is a Slater determinant, because $\rho_l^{(1)}=1$ for occupied states and $\rho_l^{(1)}=0$ for unoccupied states. That is, the density operator $\hat{\rho}_{\Psi}^{(1)}$ satisfies $\{\hat{\rho}_{\Psi}^{(1)}\}^2=\hat{\rho}_{\Psi}^{(1)}$ in the single-particle Hilbert space for a Slater determinant wave function [29].

In analogy to the expression (11) for the particle number by the σ sum and r integral of the "local" density $\rho^{(1)}(r\sigma)$, I define "local" entanglement entropy as follows,

$$S^{(1)} = \sum_{\boldsymbol{\sigma}} \int s^{(1)}(\boldsymbol{r}\boldsymbol{\sigma})d\boldsymbol{r}, \tag{14}$$

$$s^{(1)}(\boldsymbol{r}\sigma) = \sum_{l} \left[-\rho_{l}^{(1)} \log \rho_{l}^{(1)} \right] \phi_{l}^{*}(\boldsymbol{r}\sigma) \phi_{l}(\boldsymbol{r}\sigma). \tag{15}$$

Here the factor $[-\rho_l^{(1)}\log\rho_l^{(1)}]$ is contribution of the single-particle state $|l\rangle$ in $S^{(1)}$, and $\phi_l^*(\boldsymbol{r}\sigma)\phi_l(\boldsymbol{r}\sigma)$ means the density distribution in $|l\rangle$ and it is normalized as $\sum_{\sigma}\int d\boldsymbol{r}\phi_l^*(\boldsymbol{r}\sigma)\phi_l(\boldsymbol{r}\sigma)=1$. Therefore, the local entanglement entropy $s^{(1)}(\boldsymbol{r}\sigma)$ reflects spatial distributions of the important states $|l\rangle$ that contribute to the total entanglement entropy, whereas it is hardly affected by almost occupied states having $\rho_l^{(1)}\approx 1$.

3. Entanglement entropy for linear-chain α -cluster states

For a system of independent Fermions, the wave function is given by a Slater determinant and it has zero entanglement entropy, $S^{(1)} = 0$. In general, the entanglement entropy indicates how particles are entangled with other particles, and can be an indicator for many-body correlations.

In a $n\alpha$ -cluster state, the total wave function Ψ is spin and isospin symmetric and the one-body density is block diagonal with respect to σ ; $\rho^{(1)}(\mathbf{r}\sigma;\mathbf{r}'\sigma') = \rho^{(1)}(\mathbf{r};\mathbf{r}')\delta_{\sigma\sigma'}$, where the reduced matrix $\rho^{(1)}(\mathbf{r};\mathbf{r}')$ is independent to σ . Therefore, I can discuss the density matrix and the entanglement entropy with the reduced matrix in the subspace,

$$A = 4n, (16)$$

$$n = \int \rho(\mathbf{r})d\mathbf{r},\tag{17}$$

$$\rho(\mathbf{r}) = \rho^{(1)}(\mathbf{r}\sigma, \mathbf{r}\sigma), \tag{18}$$

$$S^{(1)} = 4S, \tag{19}$$

$$S^{(1)} = 4S, (19)$$

$$S = \int s(\mathbf{r})d\mathbf{r},\tag{20}$$

$$s(\mathbf{r}) = s^{(1)}(\mathbf{r}\sigma). \tag{21}$$

In the present paper, $\rho(r)$, S, and s(r) indicate the density, the total entanglement entropy, and the local entanglement entropy, respectively, defined by the reduced density matrix.

In the present 1D cluster wave functions, single-particle wave functions for x and y coordinates are common for all nucleons and give no contribution to the entanglement entropy. Therefore, I discuss only z dependence of the local density and the local entanglement by integrating x and y coordinates as

$$\rho(z) = \int \rho(\mathbf{r}) dx dy, \tag{22}$$

$$s(z) = \int s(\mathbf{r}) dx dy. \tag{23}$$

C. Model wave functions for $n\alpha$, ⁸Be, and ²⁰Ne systems

1. Wave functions for linear-chain 2α , 3α , and 4α states

For 1D-THSR wave functions of linear-chain 2α , 3α , and 4α states, the R_i integration is approximated by summation on mesh points at 1 fm intervals. To eliminate the β dependence of the c.m.m., I correct the c.m.m. by shifting the cluster position, $R_i \to R_i' = R_i - R_G$ of basis BB wave functions $(\Phi_{\rm BB}^{n\alpha})$ in $\Phi_{\rm 1D-THSR}^{n\alpha}(\beta)$ with $R_G \equiv (R_1 + \cdots + R_n)/n$. Consequently, the 1D-THSR wave function is approximated as

$$\Phi_{\text{1D-THSR}}^{n\alpha}(\beta) \to \sum_{R_1=0,\pm 1,\dots} \cdots \sum_{R_n=0,\pm 1,\dots} \exp\left\{-\sum_{i=1}^n \frac{R_i^2}{\beta^2}\right\} \Phi_{\text{BB}}^{n\alpha}(R_1',\dots,R_n'),$$
 (24)

where mesh points of the summation are truncated in a finite box $|R_i'| \le 12$ fm. The correction of c.m.m. is equivalent to replacing the β dependent c.m.m. $\Phi_G(\beta)$ in the original 1D-THSR with $\Phi_G(0)$ localized at the origin to eliminate the β dependence in the c.m.m.,

$$\Phi_{\text{1D-THSR}}^{n\alpha} = \Phi_G^z(\beta)\Phi_{\text{int}}(\beta) \to \Phi_G^z(0)\Phi_{\text{int}}(\beta), \tag{25}$$

$$\Phi_G^z(\beta) \propto \exp\left\{-\frac{A}{2b^2}X_{Gx}^2 - \frac{A}{2b^2}X_{Gy}^2 - \frac{A}{4\beta^2 + 2b^2}X_{Gz}^2\right\}$$
(26)

where X_G is the total c.m. coordinate.

2. Intrinsic wave function for ⁸Be(0⁺)

For ${}^8\mathrm{Be}(0^+)$, I use 2α -cluster wave functions. Funaki et al. have shown that ${}^8\mathrm{Be}(0^+_1)$ is well described by the three dimension (3D) THSR wave function of 2α [3, 5]. In the present paper, I consider the spherical 3D-THSR wave function, which can have 98% overlap with the exact solution of the 2α state for ${}^8\text{Be}(0_1^+)$ [24]. The definition of the 3D-THSR wave functions is explained in Appendix E.

I use the R^2 -weighted 1D-THSR wave function of 2α ,

$$\Phi_{^{8}\text{Be}}^{\text{int}}(R^{2};\beta) = \int dRR^{2} \exp\left\{-\frac{R^{2}}{2\beta^{2}}\right\} \Phi_{BB}^{2\alpha}(R_{1} = +R/2, R_{2} = -R/2), \tag{27}$$

which is regarded as the intrinsic state of the spherical 3D-THSR wave function before the angular momentum projection as

$$P^{J=0}\Phi_{^{8}\text{Be}}^{\text{int}}(R^{2};\beta) \approx \int d\mathbf{R} \exp\left\{-\frac{\mathbf{R}^{2}}{2\beta^{2}}\right\} \Phi_{\text{BB}}^{2\alpha}(\mathbf{R}_{1} = +\frac{\mathbf{R}}{2}, \mathbf{R}_{2} = -\frac{\mathbf{R}}{2}) = \frac{\Phi_{G}(0)}{\Phi_{G}(\beta)} \Phi_{^{3D\text{-THSR}}}^{2\alpha}(\beta), \tag{28}$$

where the factor $\Phi_G(0)/\Phi_G(\beta)$ is the correction of the β dependent c.m.m., and $\Phi_{3D\text{-THSR}}(\beta)$ is the spherical 3D-THSR wave function, which are described in Appendix E. In the practical calculation, the R integration in Eq. (27) is approximated by summation of mesh points at , $R = 0, 1, \dots, 24$ fm.

3. Intrinsic wave functions for $^{20}Ne(0^+)$ and $^{20}Ne(1^-)$

For $^{20}\text{Ne}(0_1^+)$ and $^{20}\text{Ne}(1_1^-)$, I use $^{16}\text{O} + \alpha$ -cluster wave functions. Zhou et al. have shown that these states of ²⁰Ne are well described by 3D-THSR wave functions of $^{16}O + \alpha$ [6, 7]. In the present paper, I consider the spherical 3D-THSR wave functions, which can have more than 98% and 99% overlaps with the exact solutions of the $^{16}O + \alpha$ states for ${}^{20}\text{Ne}(0^+)$ and ${}^{20}\text{Ne}(1^-)$ [24].

In the present paper, I fix the center position of ¹⁶O at the origin by omitting the recoil of the ¹⁶O core and consider the R^k -weighted Gaussian distribution of an α cluster around the ¹⁶O core. The intrinsic wave function of the 3D-THSR wave function of $^{16}O + \alpha$ is essentially given by the following separable form of the 1D-THSR wave function of α - (2α) on the z axis and the $(0p_x)^4(0p_y)^4$ ho shell-model wave function as

$$\Phi_{^{20}\text{Ne}}^{\text{int}}(R^k;\beta) = \mathcal{A}\left\{\Phi_{\text{ho}}\left[(0p_x)^4(0p_y)^4\right]\Phi_{\text{1D-THSR}}^{\alpha\text{-}(2\alpha)}(R^k;\beta)\right\}$$
(29)

$$\Phi_{\text{1D-THSR}}^{\alpha-(2\alpha)}(R^k;\beta) = \int dR_1 R_1^k \exp\left\{-\frac{R_1^2}{\beta^2}\right\} \Phi_{\text{BB}}^{3\alpha}(R_1, R_2 = +\varepsilon, R_3 = -\varepsilon), \tag{30}$$

where $\Phi_{\text{ho}}\left[(0p_x)^4(0p_y)^4\right]$ is the 8-nucleon wave function of the $(0p_x)^4(0p_y)^4$ ho shell-model configuration at the origin, and $\Phi_{\text{1D-THSR}}^{\alpha-(2\alpha)}(R^k;\beta)$ is the 1D-THSR α -(2 α) wave function for an α cluster with the R^k -weighted Gaussian distribution around the fixed 2α core at the origin, and ε is taken to be an enough small value. $\Phi_{^{20}\text{Ne}}^{\text{int}}(R^k;\beta)$ is regarded as the intrinsic wave function of the spherical 3D-THSR wave function for $^{20}\text{Ne}(0^+)$ and $^{20}\text{Ne}(1^-)$ in the no recoil approximation as

$$P^{J=0}\Phi_{^{20}Ne}^{int}(R^2;\beta) \approx \int d\mathbf{R}_1 \exp\left\{-\frac{\mathbf{R}_1^2}{\beta^2}\right\} \Phi_{BB}^{^{16}O-\alpha}(\mathbf{R}'=0,\mathbf{R}_1),$$
 (31)

$$P_M^{J=1}\Phi_{20\,\text{Ne}}^{\text{int}}(R^3;\beta) \approx \int d\mathbf{R}_1 R_1 Y_{1M}(\hat{\mathbf{R}}_1) \exp\left\{-\frac{\mathbf{R}_1^2}{\beta^2}\right\} \Phi_{\text{BB}}^{^{16}\text{O-}\alpha}(\mathbf{R}'=0,\mathbf{R}_1),$$
 (32)

$$\Phi_{\mathrm{BB}}^{^{16}\mathrm{O}\text{-}\alpha}(\mathbf{R}',\mathbf{R}_1) = \mathcal{A}\left[\psi_{\mathbf{R}'}^{^{16}\mathrm{O}}\psi_{\mathbf{R}_1}^{\alpha}\right]. \tag{33}$$

Here $\psi_{R'}^{^{16}\mathrm{O}}$ is the ho shell-model wave function of the p-shell closure around the position R'. In the intrinsic wave function $\Phi_{^{20}\mathrm{Ne}}^{\mathrm{int}}(R^k;\beta)$, 8 nucleons in $0p_x$ and $0p_y$ orbits give no contribution to the entanglement entropy, and therefore, I analyze the 1D-THSR wave function of α - (2α) , $\Phi_{\text{1D-THSR}}^{\alpha$ - (2α) , for ²⁰Ne. In the practical calculation, the R_1 integration in Eq. (30) is approximated by summation of mesh points, $\sum_{R=0,\pm 1,...,\pm 12 \text{ fm}}$, and $\varepsilon = 0.02 \text{ fm is used.}$

III. RESULTS

I analyze the system size (β) dependence of the entanglement entropy in 1D cluster states of $n\alpha$ and $^{16}\text{O} + \alpha$ systems. Based on the analysis of the entanglement entropy, I discuss the delocalization of clusters in the linear-chain 3α and 4α states, the 2α state for ${}^8\mathrm{Be}$, and the ${}^{16}\mathrm{O}+\alpha$ states for ${}^{20}\mathrm{Ne}$, whose intrinsic wave functions are approximately described by the 1D-THSR wave functions, $\Phi_{1\mathrm{D-THSR}}^{n\alpha}(\beta)$, $\Phi_{8\mathrm{Be}}^{\mathrm{int}}(R^2;\beta)$, and $\Phi_{1\mathrm{D-THSR}}^{\alpha-(2\alpha)}(R^k;\beta)$, respectively, with optimum β values. The optimum β values for the linear-chain 3α and 4α states are taken from Ref. [8], and those for ${}^8\mathrm{Be}(0_1^+)$, ${}^{20}\mathrm{Ne}(0^+)$, and ${}^{20}\mathrm{Ne}(1^-)$ are reduced from the results for the spherical 3D-THSR wave functions in Ref. [24].

A. Analysis of one cluster

I analyze entanglement entropy of a 1α system expressed by the 1D-THSR wave function $\Phi_{\text{1D-THSR}}^{1\alpha}(\beta)$, where an α cluster moves in the Gaussian distribution with the range β around the origin. The c.m.m. is not corrected. This system is regarded as an α cluster trapped in a ho external potential. In $\Phi_{\text{1D-THSR}}^{1\alpha}(\beta)$, α is the composite particle of 4 nucleons, but it is easy to mathematically extend the 1D-THSR wave function for a general composite particle consisting of N_f constituent particles (N_f is the particle number in the composite particle),

$$\psi_{\mathbf{R}_1}^{\alpha} = \prod_{\sigma=1}^{N_f} \phi_{\mathbf{R}_1}^{0s} \chi_{\sigma}, \tag{34}$$

where σ is the label for N_f species of particles, which are not identical to each other. Figure 1(a) shows β dependence of the entanglement entropy S defined by the reduced density matrix for a σ particle. In the small system size (β) limit, S goes to zero because the cluster is localized around the origin in the 1D-THSR wave function. With increase of the system size β , the entanglement entropy S increases. For a fixed β , S is saturated with increase of the number of constituent particles (N_f).

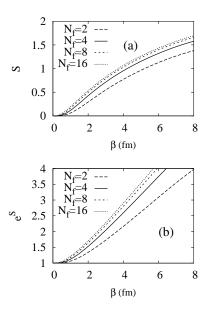


FIG. 1: (a) β dependence of entanglement entropy S for a cluster consisting of N_f particles for $N_f = 2, 4, 8$, and 16. S defined by the reduced density matrix for a fixed species σ is shown. (b) Same as (a) but β dependence of $\exp(S)$.

If the one-body density is fragmented equally into m states, $S = \log m$ (m is the number of states). For instance, in the case that the one-body density is fragmented equally into two states, $S = \log 2 = 0.693$. It is naively expected that the number of independent states that contribute to the entanglement entropy S is proportional to β/b (the system size divided by the cluster size). Provided that the one-body density is fragmented equally into these states, $\exp(S)$ should have a linear dependence on the system size β . As shown in Fig. 1(b), $\exp(S)$ is a almost linear function of β , supporting the naive expectation.

Spatial distributions of local entanglement entropy s(z) and density $\rho(z)$ in the 1D-THSR wave function for the 1α system is shown in Fig. 2. In case of the system size as small as $\beta=1$ fm, where an α cluster is well localized around the origin as shown by the density almost the same as that for a fixed α cluster, s(z) is quite small. As β increases, delocalization of cluster develops and s(z) increases in particular in low-density regions at the surface. s(z) is relatively suppressed at the high-density region near the origin.

The analysis of one-cluster systems suggests that the entanglement entropy is enhanced in a low-density cluster gas having a relatively larger system size than the cluster size. The entanglement entropy S and the local entropy S(z) can be a good measure for the delocalization of cluster.

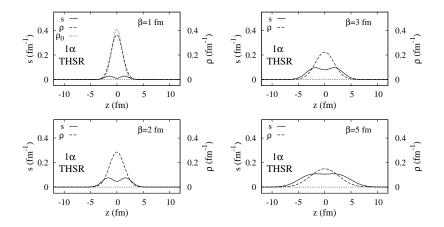


FIG. 2: Spatial distributions of local entanglement entropy s(z) and density $\rho(z)$ in the 1D-THSR wave function for the 1α system with $\beta = 1, 2, 3$, and 5 fm. The density $\rho_0(z)$ of a localized α for the $\beta = 0$ limit is also shown in the left top panel.

B. Linear-chain states of $n\alpha$ systems

I analyze entanglement entropy of the 1D-THSR wave functions for the linear-chain 2α , 3α , and 4α states. Figure 3 shows the system size (β) dependence of S. Similarly to the 1α system discussed previously, S increases as the system size β increases. In Fig. 4, entanglement entropy per α cluster, S/n, is plotted as a function of β . If α -cluster motion is not affected by other α clusters, S should be proportional to the number (n) of α clusters. S/n is somewhat suppressed as n increases because of the Pauli blocking effect between α clusters, which comes from the antisymmetrization effect between nucleons in different α clusters. That is, delocalization of α clusters is suppressed because the effective system size for the α -cluster motion is reduced by the Pauli blocking effect.

The Pauli blocking effect should be relatively strong in the inner high-density region rather than at the low-density surface region. To see the contribution of the low-density tail part of the α -cluster Gaussian distribution to the entanglement entropy, I calculate S of the "tail-cut" 1D-THSR wave functions with no outer tail, where the basis wave functions are truncated as $|R_i'| \leq \beta$ by cutting off the basis wave functions in the $|R_i'| > \beta$ region for the tail component. S of the tail-cut 1D-THSR wave functions indicates the contribution of the inner part in the total entropy, whereas, the difference of S between the tail-cut wave functions and the original ones approximately corresponds to the contribution of the tail part. S of the tail-cut 1D-THSR wave functions shown by dashed lines in Fig. 3 is much smaller than that of the original 1D-THSR wave functions in 3α and 4α systems, indicating the significant contribution of the tail component in S. The tail contribution in the total entanglement entropy is larger than 50% in the $\beta \leq 4$ fm region for 3α and in the $\beta \leq 6$ fm region for 4α . For the same β value, the contribution of the inner part in S is relatively small in 4α than in 3α because of the Pauli blocking effect.

Figure 5 shows local entanglement entropy s(z) of 2α , 3α , and 4α for the system size $\beta=2$, 5, and 8 fm. In case of the small system size as $\beta=2$ fm, s(z) is almost zero, which indicates no delocalization of α clusters. As β increases, s(z) increases and shows a broader spatial distribution than the density distribution. s(z) is relatively suppressed in the inner high-density region and enhanced in the low-density region at the surface. It means that the significant contribution in the entanglement entropy originates in more broadly distributed orbits than the system size. Comparing the result for a given β between 2α , 3α , and 4α systems, the larger n (the number of α clusters) system shows more suppression of s(z) in the inner region than the smaller n system because of the Pauli blocking effect.

Let us consider correspondence of the present result with the linear-chain 3α and 4α states in ¹²C and ¹⁶O predicted by Suhara *et al.* In Ref. [8], they have applied the generator coordinate method (GCM) to the linear-chain 3α and 4α states using effective nuclear forces to exactly solve 1D dynamics of 3α and 4α , and obtained the energy minimum wave functions in the model space of linear configurations. It has been shown that the wave functions of the linear 3α and 4α states obtained with the GCM calculations have large overlap with the 1D-THSR wave functions. The optimum

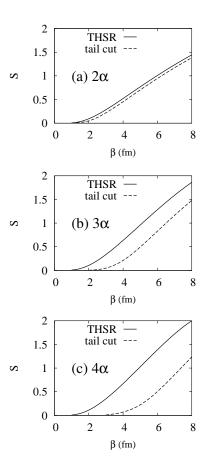


FIG. 3: β dependence of entanglement entropy S of the 1D-THSR wave functions for 2α , 3α , and 4α (solid lines). S of the tail-cut 1D-THSR wave functions is also shown (dashed lines).

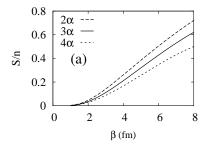


FIG. 4: Entanglement entropy per α cluster, S/n, plotted as a function of β of the 1D-THSR wave functions for 2α , 3α , and 4α .

parameters of the 1D-THSR wave functions are $\beta=5.1$ fm and $\beta=8.2$ fm for the 0^+ linear-chain states of 3α and 4α , respectively. Looking at the result of corresponding wave functions, $\Phi_{1\text{D-THSR}}^{3\alpha}(\beta=5\text{ fm})$ and $\Phi_{1\text{D-THSR}}^{4\alpha}(\beta=8\text{ fm})$, shown in Figs. 3 and 5, it is found that the entanglement entropy is generated by the delocalization of α clusters. In particular, in the linear-chain 4α states with the large system size as $\beta=8\text{ fm}$, s(z) is broadly distributed with significant amplitude. In both cases of the linear-chain 3α and 4α states, the tail contribution is significantly large as shown in the comparison of S between the tail-cut 1D-THSR and the original 1D-THSR wave functions in Fig. 3. In the 3α state with $\beta=5$ fm, the tail contribution is as large as $\sim 50\%$ of the total entropy. In Fig. 6, spatial distributions of s(z) and $\rho(z)$ in the tail-cut 1D-THSR wave function of 3α with $\beta=5$ fm and those of 4α with $\beta=8$ fm are shown by solid and dashed lines compared with those in the original 1D-THSR wave functions shown by

dash-dotted and dotted lines. For the 3α state with $\beta=5$ fm, the tail-cut 1D-THSR wave function shows the overall reduction of s(z) compared with the original 1D-THSR, indicating that the delocalization of α clusters occurs mainly in the low-density region at the surface. In other words, about half of the total entanglement entropy is generated due to the small difference in the tail component of the α distribution of the original 1D-THSR wave function from the tail-cut 1D-THSR one. In the 4α state with $\beta=8$ fm, the tail-cut 1D-THSR wave function shows some reduction of s(z) at the surface region, but a significant amplitude of s(z) still remains in the inner region even after the tail cut. It means that, in the 4α state, the delocalization of α clusters occurs also in the inner region as well as at the surface region.

I also demonstrate s(z) and $\rho(z)$ in the localized cluster limit of the linear-chain 3α and 4α states given by the BB wave functions, where each α cluster is localized at a certain position R_i . They corresponds to the conventional linear-chain states. I set the α -cluster positions R_i on the z axis at equal intervals d=3.8 fm in the 3α system and d=4 fm in the 4α system so as to give density $(\rho(z))$ peak positions similar to those of the corresponding 1D-THSR wave functions, $\Phi_{1\mathrm{D-THSR}}^{3\alpha}(\beta=5\,\mathrm{fm})$ and $\Phi_{1\mathrm{D-THSR}}^{4\alpha}(\beta=8\,\mathrm{fm})$. In Fig. 6, s(z) and $\rho(z)$ in these BB wave functions for the conventional linear-chain states are compared with those of the 1D-THSR wave functions. s(z) in the BB wave functions completely vanishes because S is trivially zero for a single Slater determinant. This result indicates that local entanglement entropy s(z) shows the prominent difference between the localized and delocalized wave functions for the linear-chain 3α and 4α states even though the difference in density is not so remarkable, in particular, in the 3α state. It is concluded that both S and s(z) are sensitive to the delocalization of α clusters.

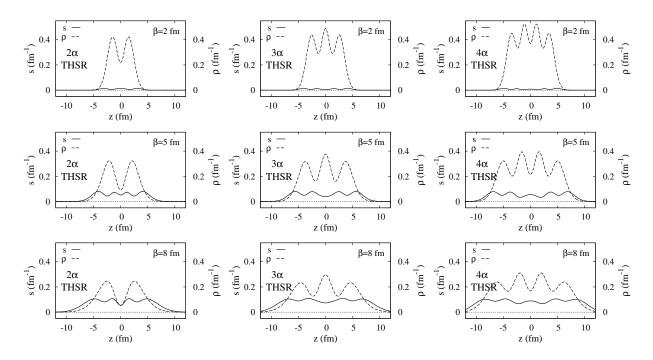


FIG. 5: Spatial distributions of local entanglement entropy s(z) and density $\rho(z)$ in the 1D-THSR wave functions of 2α , 3α , and 4α systems with $\beta=2, 5$, and 8 fm.

C. $\alpha + \alpha$ for ⁸Be

As pointed out by Funaki et al., the exact 2α wave function for ${}^8\mathrm{Be}(0_1^+)$ is well described by the 3D-THSR wave function [3, 5]. In the present paper, I use the R^2 -weighted 1D-THSR wave function, $\Phi_{^8\mathrm{Be}}^{\mathrm{int}}(\beta)$, in Eq. (27) as the intrinsic wave function of the spherical 3D-THSR wave function. The parameter $\beta=3.3$ fm is reduced from the optimum parameter B=4.77 fm with b=1.36 fm of the spherical 3D-THSR wave function for ${}^8\mathrm{Be}(0_1^+)$ taken from Ref. [24], using the relation $B^2=b^2+2\beta^2$ and the scaling b=1.36 fm $\to 1.376$ fm. (The parameter B here is originally labeled by " σ " in Ref. [24].)

Figure 7(a) shows β dependence of the entanglement entropy S of $\Phi_{\rm sBe}^{\rm int}(\beta)$. For comparison, S of the R^0 -weighted 1D-THSR wave function is also shown. At the optimized parameter $\beta = 3.3$ fm for $^8{\rm Be}(0_1^+)$, S = 0.6 is generated

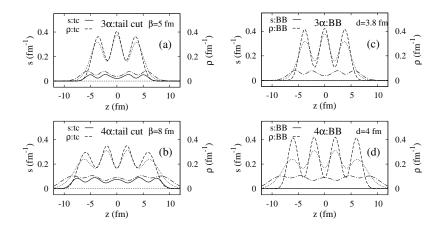


FIG. 6: Spatial distributions of local entanglement entropy s(z) and density $\rho(z)$ in (a) the tail-cut 1D-THSR wave function of 3α with $\beta=5$ fm, (b) the tail-cut 1D-THSR wave function of 4α with $\beta=8$ fm, (c) the BB wave function of 3α with the interval d=3.8 fm, and (d) the BB wave function of 4α with d=4 fm. s(z) and $\rho(z)$ in the original 1D-THSR wave functions of 3α with $\beta=5$ fm are also shown by dash-dotted and dotted lines, respectively, in (a) and (c), and those of 4α with $\beta=8$ fm are shown in (b) and (d).

by the delocalization of α clusters. Spatial distributions of local entanglement entropy (s(z)) and density $(\rho(z))$ in $\Phi_{^8\mathrm{Be}}^{\mathrm{int}}(\beta=3.3\ \mathrm{fm})$ are shown in Fig. 7(b).

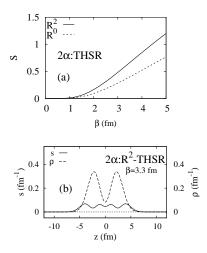


FIG. 7: (a) β dependence of entanglement entropy S of the R^2 -weighted 1D-THSR $\Phi_{^8\mathrm{Be}}^{\mathrm{int}}(\beta)$ of 2α . That of the normal (R^0 -weighted) 1D-THSR of 2α is also shown. (b) Spatial distributions of local entanglement entropy s(z) and density $\rho(z)$ in $\Phi_{^8\mathrm{Be}}^{\mathrm{int}}(\beta)$ with $\beta=3.3$ fm for $^8\mathrm{Be}(0_1^+)$.

D. 16 O+ α for 20 Ne

As shown by Zhou et al., $^{20}\mathrm{Ne}(0_1^+)$ and $^{20}\mathrm{Ne}(1_1^-)$ are well described by the 3D-THSR wave functions [6, 7]. As approximated intrinsic wave functions of the spherical 3D-THSR wave functions for $^{20}\mathrm{Ne}(0_1^+)$ and $^{20}\mathrm{Ne}(1_1^-)$, I use the R^2 - and R^3 -weighted 1D-THSR wave functions, $\Phi_{1D-\mathrm{THSR}}^{\alpha-(2\alpha)}(R^k;\beta)$ in Eq. (30), respectively. For comparison, I also use localized cluster wave functions given by following parity projected BB wave functions with the fixed α -(2 α) distance

d,

$$\Phi_{\rm BB}^{\alpha - (2\alpha), \pm}(d) = \Phi_{\rm BB}^{3\alpha}(R_1 = d, R_2 = +\varepsilon, R_3 = -\varepsilon)
\pm \Phi_{\rm BB}^{3\alpha}(R_1 = -d, R_2 = +\varepsilon, R_3 = -\varepsilon).$$
(35)

 $\Phi_{\rm BB}^{\alpha-(2\alpha),\pm}(d)$ is given by the linear combination of two Slater determinants, and in the large d limit, it has $S = \log 2$. For the 1D-THSR α - (2α) wave functions, the optimum parameters $\beta = 2.0$ fm and $\beta = 2.6$ fm for $^{20}{\rm Ne}(0_1^+)$ and $^{20}{\rm Ne}(1_1^-)$ are reduced from B = 2.39 fm and B = 2.97 fm, respectively for the spherical 3D-THSR wave functions with b = 1.46 fm in Ref. [24] using the relation $B^2 = \beta^2 + b^2/2$ and the scaling b = 1.46 fm $\rightarrow 1.376$ fm. For the positive- and negative-parity projected BB wave functions, I use the optimum parameters d = 3.05 fm and d = 3.85 fm taken from Ref. [24], respectively.

Fig. 8 shows β dependence of S of the 1D-THSR wave function, $\Phi_{\text{1D-THSR}}^{\alpha-(2\alpha)}(R^k;\beta)$ for ^{20}Ne , and also shows d dependence of S for the BB wave function, $\Phi_{\text{BB}}^{\alpha-(2\alpha),\pm}(d)$ for the localized cluster wave function. For comparison, I also show the result of the R^0 -weighted 1D-THSR wave function of an α cluster with and without the 2α core. In the R^2 -weighted 1D-THSR wave function of α - (2α) , S is zero at $\beta \to 0$ and rapidly increases in $\beta \lesssim 1$, and it gradually increases in the $\beta \gtrsim 1$ region. In the R^3 -weighted 1D-THSR wave function, S is finite even at $\beta \to 0$ because $\Phi_{\text{1D-THSR}}^{\alpha-(2\alpha)}(R^3; \beta \to 0)$ is equivalent to the shell model limit wave function having 3 nucleons in the sd shell and a nucleon in the pf shell, which has $S = -\frac{3}{4}\log\frac{3}{4} - \frac{1}{4}\log\frac{1}{4} = 0.562$. With increase of β , S of $\Phi_{\text{1D-THSR}}^{\alpha-(2\alpha)}(R^3; \beta)$ becomes close to that of $\Phi_{\text{1D-THSR}}^{\alpha-(2\alpha)}(R^2;\beta)$. In case of the positive-parity projected BB wave function, S rapidly increases with the increase of d and it becomes constant $S = \log 2$ in the $d \gtrsim 3$ fm region. The negative-parity projected BB wave function shows small d dependence of S as S=0.562 at $d\to 0$ and $S=\log 2$ in the large d region. $S=\log 2$ is generated in both the positive- and negative-parity projected BB wave functions with a large d, because the α -cluster wave functions are separated into two parts in z > 0 and z < 0, which have almost no overlap with each other. This indicates that even the localized cluster wave functions can have the finite entanglement entropy $S = \log 2$ by the parity projection. In comparison of S between the 1D-THSR and BB wave functions, it is found that the entanglement entropy $S \sim \log 2$ generated in the 1D-THSR wave functions of α -(2 α) with $\beta \lesssim 1.5$ fm does not originate in the delocalization of the α cluster but it is understood by the effect of parity projection. With further increase of β in the 1D-THSR wave functions, S increases due to the delocalization of the α cluster and it becomes larger than log 2. Let us consider correspondence of the present result with ${}^{20}\text{Ne}(0_1^+)$ and ${}^{20}\text{Ne}(1_1^-)$. As mentioned previously, $\Phi_{\text{1D-THSR}}^{\alpha-(2\alpha)}(R^2; \beta = 2.0 \text{ fm})$ and $\Phi_{\text{1D-THSR}}^{\alpha-(2\alpha)}(R^3; \beta = 2.6 \text{ fm})$ correspond to the intrinsic wave functions of $^{20}\text{Ne}(0_1^+)$ and $^{20}\text{Ne}(1_1^-)$ described by the spherical 3D-THSR wave functions, respectively. $\Phi_{\text{BB}}^{\alpha-(2\alpha),+}(d = 3.05 \text{ fm})$ and $\Phi_{\rm BB}^{\alpha-(2\alpha),-}(d=3.85~{\rm fm})$ correspond to the optimized BB wave functions for $^{20}{\rm Ne}(0_1^+)$ and $^{20}{\rm Ne}(1_1^-)$. Figure 9 shows spatial distributions of local entanglement entropy (s(z)) and density $(\rho(z))$ in these wave functions. For ²⁰Ne(0₁⁺), $\Phi_{\text{1D-THSR}}^{\alpha-(2\alpha)}(R^2; \beta = 2.0 \text{ fm})$ and $\Phi_{\text{BB}}^{\alpha-(2\alpha),+}(d = 3.05 \text{ fm})$ show similar distributions of s(z) and $\rho(z)$ to each other. s(z) almost vanishes in the $-2 \le z \le 2$ fm region because of the Pauli blocking from the core and it has amplitude only at surface regions. $\Phi_{\text{1D-THSR}}^{\alpha-(2\alpha)}(R^2; \beta = 2.0 \text{ fm})$ and $\Phi_{\text{BB}}^{\alpha-(2\alpha),+}(d = 3.05 \text{ fm})$ have the total entanglement entropy S = 0.76 and S = 0.67, respectively. They are close to $\log 2$, which is generated mainly just by the parity projection, indicating that the delocalization of the α cluster is weak in the intrinsic state of ²⁰Ne(0₁⁺). For ²⁰Ne(1₁⁻), $\Phi_{\text{1D-THSR}}^{\alpha-(2\alpha)}(R^3; \beta = 2.6 \text{ fm})$ shows a broader distribution of s(z) in the outer tail part than that of $\Phi_{\text{BB}}^{\alpha-(2\alpha),-}(d=3.85 \text{ fm})$. $\Phi_{\text{1D-THSR}}^{\alpha-(2\alpha)}(R^3; \beta = 2.6 \text{ fm})$ has the total entropy S=0.90 larger than S=0.69 of $\Phi_{\rm BB}^{\alpha-(2\alpha),-}(d=3.85 \text{ fm})$. It means that, the entropy is somewhat generated by the delocalization of the α cluster in addition to $S = \log 2$ from the parity projection. This additional entanglement entropy by the delocalization comes from a low-density outer tail of the wave function. That is, the delocalization of an α cluster occurs in the low-density tail part.

IV. SUMMARY AND OUTLOOK

In order to investigate delocalization of clusters in the 1D cluster systems, I proposed a method of analysis using entanglement entropy defined by the one-body density matrix. I studied the entanglement entropy of the 1D cluster states of $n\alpha$ and $^{16}\text{O} + \alpha$ systems, and discussed the delocalization of clusters in the intrinsic wave functions of the linear-chain 3α - and 4α -cluster states, $^{8}\text{Be}(0_{1}^{+})$, and $^{20}\text{Ne}(0_{1}^{+},1_{1}^{-})$. I investigated the entanglement entropy of the 1D-THSR wave functions and compared it with that of the BB cluster wave functions, and showed clear differences in the entanglement entropy between localized cluster wave functions and delocalized cluster wave functions.

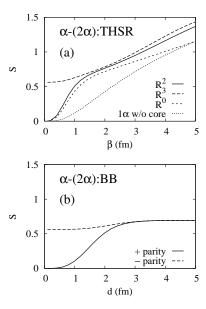


FIG. 8: (a) β dependence of entanglement entropy S of the R^k -weighted 1D-THSR wave functions $\Phi_{\text{1D-THSR}}^{\alpha-(2\alpha)}(R^k;\beta)$ of α -(2 α) and the 1D-THSR wave function $\Phi_{\text{1D-THSR}}^{1\alpha}(\beta)$ of 1α without the 2α core, and (b) d dependence of S of the parity projected BB wave functions $\Phi_{\text{BB}}^{\alpha-(2\alpha),\pm}(d)$.

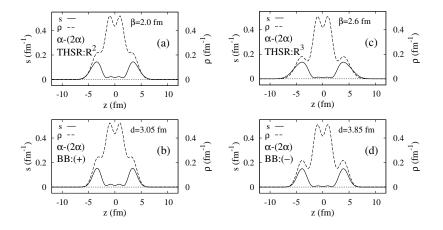


FIG. 9: Spatial distributions of local entanglement entropy s(z) and density $\rho(z)$ in (a) $\Phi_{\text{1D-THSR}}^{\alpha-(2\alpha)}(R^2;\beta)$ with $\beta=2.0$ fm for $^{20}\text{Ne}(0_1^+)$, (b) $\Phi_{\text{BB}}^{\alpha-(2\alpha),+}(d)$ with d=3.05 fm, (c) $\Phi_{\text{1D-THSR}}^{\alpha-(2\alpha)}(R^3;\beta)$ with $\beta=2.6$ fm for $^{20}\text{Ne}(1_1^-)$, and (d) $\Phi_{\text{BB}}^{\alpha-(2\alpha),-}(d)$ with d=3.85 fm.

I calculated the entanglement entropy of the 1D-THSR wave functions for linear-chain 2α , 3α , and 4α systems, and discuss the dependences on the system size (β) and the number (n) of α clusters. With increase of the system size β , the entanglement entropy increases as the delocalization of α clusters develops. With increase of the number of α clusters, the entanglement entropy per α cluster decreases because of the Pauli blocking effect between clusters. In order to clarify the spatial regions where the entanglement entropy is generated by the delocalization, I defined the local entanglement entropy s(z). I found that the entanglement entropy is generated in the low-density part whereas it is relatively suppressed in the high-density part, indicating that the delocalization of clusters occurs dominantly in the low-density region but it is suppressed in the high-density region because of the Pauli blocking effect between clusters.

Moreover, I discussed the delocalization of α clusters in the linear-chain 3α and 4α states predicted in 12 C and 16 O by Suhara *et al.* [8] based on the analysis of the entanglement entropy. In the linear-chain 3α state, the delocalization of clusters occurs dominantly in the low-density tail region while it is relatively suppressed in the inner region because

of the Pauli blocking effect. In the linear-chain 4α state having the significantly larger system size than the linear-chain 3α state, the delocalization occurs in the whole system.

I also analyzed the entanglement entropy of the R^k -weighted 1D-THSR wave functions of 2α and α - (2α) systems, which correspond to the intrinsic wave functions of the cluster states in ${}^8\text{Be}(0^+_1)$, ${}^{20}\text{Ne}(0^+_1)$, and ${}^{20}\text{Ne}(1^-_1)$. In ${}^8\text{Be}(0^+_1)$, the entanglement entropy is generated because of the delocalization of clusters. In ${}^{20}\text{Ne}(0^+_1)$ and ${}^{20}\text{Ne}(1^-_1)$, the entanglement entropy is strongly suppressed in the inner region because of the Pauli blocking from the core. The entanglement entropy is generated at the surface region mainly because of the parity projection. In particular, in ${}^{20}\text{Ne}(0^+_1)$, the delocalization of the α cluster is weak and gives a minor contribution to the total entanglement entropy.

The present result shows that the entanglement entropy is generated by the delocalization of clusters. The entanglement entropy is sensitive to the localization and delocalization of clusters and it can be a good measure to discuss the delocalization of clusters in 1D cluster states. In the present paper, I investigated the entanglement entropy only in 1D cluster wave functions, which are regarded as intrinsic states of 3D nuclear systems, and discuss the delocalization in the 1D motion, i.e., the delocalization in radial motion of clusters. Zero entanglement entropy in the BB wave functions for localized cluster wave functions indicates that clusters are not delocalized but localized in the intrinsic systems. However, I should comment that, in realistic 3D wave functions, the 1D cluster wave functions should be projected on to the angular-momentum eigen states. The angular momentum projection to 0^+ states from the 1D cluster wave functions usually causes the delocalization of clusters in angle motion. In that sense, the localized cluster wave functions may contain implicitly the delocalization in the angle motion even though the delocalization does not occur in the radial motion. The localization of clusters in intrinsic states, for which the delocalization occurs in angle motion by the angular momentum projection, is regarded as a kind of strong cluster correlations

In principle, the present method with entanglement entropy can be extended to 3D cluster systems, but it is practically not easy to calculate entanglement entropy in 3D because high dimensional single-particle bases are needed in diagolization of the one-body density matrix in 3D. Moreover, as explained in Appendix F, the entanglement entropy in 3D systems should have strong dependence on the single-particle angular momentum j at the Fermi surface, because considerable entanglement entropy is generated in the angular momentum projection, which might wash out a pure contribution from the delocalization of clusters in the entanglement entropy.

Acknowledgments

The author would like to thank H. Iida and T. Suhara for helpful discussions. The calculations of this work have been done using computers at Yukawa Institute for Theoretical Physics, Kyoto University. This work was supported by JSPS KAKENHI Grant No. 26400270.

Appendix A: Density matrix

I describe density matrices. For details of the one-body density matrix, the readers are referred to, for example, Ref. [29]. An A-body density matrix for a wave function $\Psi(\mathbf{r}\sigma, \mathbf{r}_2\sigma_2, \dots, \mathbf{r}_A\sigma_A)$ for an A-nucleon system is defined in the coordinate space as

$$\rho^{(A)}(\mathbf{r}_{1}\sigma_{1}, \mathbf{r}_{2}\sigma_{2}, \dots, \mathbf{r}_{A}\sigma_{A}; \mathbf{r}'_{1}\sigma'_{1}, \mathbf{r}'_{2}\sigma'_{2}, \dots, \mathbf{r}'_{A}\sigma'_{A})
= A!\Psi^{*}(\mathbf{r}'_{1}\sigma'_{1}, \mathbf{r}'_{2}\sigma'_{2}, \dots, \mathbf{r}'_{A}\sigma'_{A})\Psi(\mathbf{r}_{1}\sigma_{1}, \mathbf{r}_{2}\sigma_{2}, \dots, \mathbf{r}_{A}\sigma_{A})
= \langle \Psi | a^{\dagger}(\mathbf{r}'_{1}\sigma'_{1})a^{\dagger}(\mathbf{r}'_{2}\sigma'_{2}) \cdots a^{\dagger}(\mathbf{r}'_{A}\sigma'_{A})a^{\dagger}(\mathbf{r}_{A}\sigma_{A}) \cdots a^{\dagger}(\mathbf{r}_{2}\sigma_{2})a^{\dagger}(\mathbf{r}_{1}\sigma_{1}) | \Psi \rangle,$$
(A1)

where $a^{\dagger}(r\sigma)$ and $a(r\sigma)$ are creation and annihilation operators of a nucleon at the position r with the spin-isospin $\sigma = p \uparrow, p \downarrow, n \uparrow, n \downarrow$. Ψ is normalized as $\langle \Psi | \Psi \rangle = 1$. $\rho^{(A)}$ is regarded as the matrix element of the A-body density operator $\hat{\rho}_{\Psi}^{(A)} = |\Psi\rangle\langle\Psi|$. The one-body density matrix is defined in the coordinate space as

$$\rho^{(1)}(\boldsymbol{r}\sigma;\boldsymbol{r}'\sigma') = \langle \Psi^{(A)} | a^{\dagger}(\boldsymbol{r}'\sigma') a(\boldsymbol{r}\sigma) | \Psi^{(A)} \rangle. \tag{A2}$$

 $\rho^{(1)}$ is given by the trace of the A-body density matrix

$$\rho^{(1)}(\boldsymbol{r}\sigma;\boldsymbol{r}'\sigma') = A \sum_{\sigma_2,\dots,\sigma_A} \int d\boldsymbol{r}_2 \dots d\boldsymbol{r}_A \Psi^*(\boldsymbol{r}'\sigma',\boldsymbol{r}_2\sigma_2,\dots,\boldsymbol{r}_A\sigma_A) \Psi(\boldsymbol{r}\sigma,\boldsymbol{r}_2\sigma_2,\dots,\boldsymbol{r}_A\sigma_A)$$

$$= A \operatorname{Tr}_2 \dots \operatorname{Tr}_A \rho^{(A)}, \tag{A3}$$

which is also called reduced density matrix. The one-body density matrix is regarded as the matrix element of the one-body density operator $\hat{\rho}_{\Psi}^{(1)}$ for the wave function $\Psi^{(A)}$,

$$\rho^{(1)}(\boldsymbol{r}\sigma;\boldsymbol{r}'\sigma') = \langle \boldsymbol{r}\sigma|\hat{\rho}_{\Psi}^{(1)}|\boldsymbol{r}'\sigma'\rangle,\tag{A4}$$

and I get

$$\rho^{(1)}(\boldsymbol{r}\sigma;\boldsymbol{r}'\sigma') = \sum_{pq} \varphi_p(\boldsymbol{r}\sigma)\rho_{pq}^{(1)}\varphi_q^*(\boldsymbol{r}'\sigma')$$

$$= \sum_{pq} \langle \boldsymbol{r}\sigma|p\rangle\rho_{pq}^{(1)}\langle q|\boldsymbol{r}'\sigma'\rangle, \tag{A5}$$

where

$$\rho_{pq}^{(1)} = \langle \Psi^{(A)} | c_q^{\dagger} c_p | \Psi^{(A)} \rangle \tag{A6}$$

is the matrix element of the one-body density operator $\hat{\rho}_{\Psi}^{(1)}$ in arbitrary orthonormal bases. $\hat{\rho}_{\Psi}^{(1)}$ is a Hermitian single-particle operator and it has the form

$$\hat{\rho}_{\Psi}^{(1)} = \sum_{pq} |p\rangle \rho_{pq}^{(1)} \langle q|. \tag{A7}$$

The density matrix can be diagonalized by a unitary transformation of single-particle bases

$$(D^{\dagger} \rho^{(1)} D)_{ll'} = \rho_l^{(1)} \delta_{ll'}, \tag{A8}$$

$$a_l^{\dagger} = \sum_{l'} D_{l'l} c_{l'}^{\dagger}, \tag{A9}$$

where

$$\rho_l^{(1)} = \langle \Psi^{(A)} | a_l^{\dagger} a_l | \Psi^{(A)} \rangle, \tag{A10}$$

$$0 \le \rho_l^{(1)} \le 1 \tag{A11}$$

is the eigen value of the density matrix and means the occupation number of the single-particle state $|l\rangle$ in the wave function $\Psi^{(A)}$. In the coordinate space, the diagonal element $\rho^{(1)}(\boldsymbol{r}\sigma) = \rho^{(1)}(\boldsymbol{r}\sigma,\boldsymbol{r}\sigma)$ of the density matrix is the one-body density of $\sigma = p \uparrow, p \downarrow, n \uparrow, n \downarrow$ nucleons at the position \boldsymbol{r} , and it is expressed in the bases $|l\rangle$ as,

$$\rho^{(1)}(\boldsymbol{r}\sigma) = \sum_{l} \rho_{l}^{(1)} \phi_{l}^{*}(\boldsymbol{r}\sigma) \phi_{l}(\boldsymbol{r}\sigma). \tag{A12}$$

The trace of the density matrix $\rho^{(1)}$ equals to the particle number:

$$A = \text{Tr}\rho^{(1)} = \sum_{p} \rho_{pp}^{(1)} = \sum_{l} \rho_{l}^{(1)} = \sum_{\sigma} \int \rho^{(1)}(r\sigma)dr.$$
(A13)

Appendix B: Entanglement entropy

The von Neumann entropy of an A-particle system is defined by the A-body density matrix as

$$S^{(A)} = -\operatorname{Tr}\rho^{(A)}\log\rho^{(A)},\tag{B1}$$

and trivially $S^{(A)}=0$ for the pure state $|\Psi\rangle$ because $\left\{\rho^{(A)}\right\}^2=\rho^{(A)}$.

The entanglement entropy is defined by the one-body density matrix as

$$S^{(1)} = -\text{Tr}\rho^{(1)}\log\rho^{(1)} = -\sum_{l}\rho_{l}^{(1)}\log\rho_{l}^{(1)}.$$
 (B2)

Note that the entanglement entropy can be defined by the general A'-body density matrix for $A' \leq A-1$ which is obtained by partial trace of the complete A-body density matrix for some degrees of freedom, but in the present paper, I only consider the entanglement entropy for the one-body density matrix. The entanglement entropy is zero if and only if a wave function $|\Psi^{(A)}\rangle$ can be written by a Slater determinant because $\rho_l^{(1)}=1$ or 0 for a Slater determinant as $\rho_l^{(1)}=1$ for occupied single-particle states and $\rho_l^{(1)}=0$ for unoccupied states. It is equivalent to the following theorem: A wave function $|\Psi^{(A)}\rangle$ is a Slater determinant if and only if the corresponding density operator $\hat{\rho}_{\Psi}^{(1)}$ satisfies $\{\hat{\rho}_{\Psi}^{(1)}\}^2=\hat{\rho}_{\Psi}^{(1)}$ in the single-particle Hilbert space [29]. It means that, for the ideal case of an uncorrelated Fermion system that the wave function is given by a Slater determinant, the system has exactly zero entanglement entropy, $S^{(1)}=0$. $S^{(1)}$ is finite only if a system contains many-body correlations beyond the expression of a single Slater determinant. It indicates that the entanglement entropy can be an indicator for many-body correlations.

In the present paper, I define local entanglement entropy and analyze spatial distribution of the entanglement entropy. In analogy to the expression of the particle number by the σ sum and r integral of the density $\rho^{(1)}(r\sigma)$, I define the local entanglement entropy as follows,

$$S^{(1)} = \sum_{\sigma} \int s^{(1)}(\boldsymbol{r}\sigma)d\boldsymbol{r}, \tag{B3}$$

$$s^{(1)}(\boldsymbol{r}\sigma) = \sum_{l} \left[-\rho_{l}^{(1)} \log \rho_{l}^{(1)} \right] \phi_{l}^{*}(\boldsymbol{r}\sigma) \phi_{l}(\boldsymbol{r}\sigma). \tag{B4}$$

 $\phi_l^*(\boldsymbol{r}\sigma)\phi_l(\boldsymbol{r}\sigma)$ means the density distribution in the state $|l\rangle$ and normalized as $\sum_{\sigma}\int\phi_l^*(\boldsymbol{r}\sigma)\phi_l(\boldsymbol{r}\sigma)d\boldsymbol{r}=1$, and the factor $[-\rho_l^{(1)}\log\rho_l^{(1)}]$ is the contribution of the state $|l\rangle$ in the total entanglement entropy $S^{(1)}$. Therefore, $s^{(1)}(\boldsymbol{r}\sigma)$ reflects spatial distributions of the important states $|l\rangle$ that contribute to the total entanglement entropy. Note that s(z) is not quantity determined only by local information at the position z.

Appendix C: Entanglement entropy for correlated and uncorrelated systems in a toy model

Let us consider correlated and uncorrelated wave functions in a simple toy model of an A particle system. For simplicity, A particles are assumed to be distinguishable and stay on sites in a space. The number of available sites (single-particle states) is N_s and I use the label k_j for the jth single-particle states. Each particle can occupy one of single-particle states, k_j ($j=1,\ldots,N_s$). A wave function Ψ of an A-body state is expressed by a linear combination of direct products as

$$\Psi(1,2,\ldots,A) = \sum_{\alpha_1} \sum_{\alpha_2} \cdots \sum_{\alpha_A} C(\alpha_1,\alpha_2,\ldots,\alpha_A) \phi_{\alpha_1}(1) \phi_{\alpha_2}(2) \cdots \phi_{\alpha_A}(A), \tag{C1}$$

where $\alpha_i = k_1, k_2, \dots, k_{N_s}$, and $C(\alpha_1, \dots, \alpha_A)$ is normalized as $|\langle \Psi(1, 2, \dots, A) | \Psi(1, 2, \dots, A) \rangle|^2 = 1$.

Let us first consider uncorrelated systems. If a state is an ideal state of independent particles, the wave function can be written by a simple product of single-particle wave functions

$$\Psi(1, 2, \dots, A) = \psi_1(1)\psi_2(2)\cdots\psi_A(A), \tag{C2}$$

$$\psi_i(i) = \sum_{\alpha = k_1, k_2, \dots, k_{N_s}} c_i(\alpha) \phi_\alpha(i)$$
 (C3)

and I get $S^{(1),i}=0$ because the one-body density operator for the ith particle is given as $\hat{\rho}_{\Psi}^{(1),i}=|\psi_i\rangle\langle\psi_i|$ and obviously satisfies $\{\hat{\rho}_{\Psi}^{(1),i}\}^2=\hat{\rho}_{\Psi}^{(1),i}$. (Here $\rho^{(1),i}$ is the reduced one-body density matrix defined in subspace for the ith particle, and the entanglement entropy $S^{(1),i}$ is defined by $\rho^{(1),i}$.) Let us consider the state of free particles in zero momentum that all particles move freely in the whole system with an equal weight. The wave function is given as

$$\Psi(1,2,\ldots,A) = \frac{1}{N_s^{A/2}} \prod_{i=1}^{A} \left[\phi_{k_1}(i) + \phi_{k_2}(i) + \cdots + \phi_{k_{N_s}}(i) \right].$$
 (C4)

The wave function has $S^{(1),i} = 0$. Another example is a "localized cluster" system of a cluster, where all particles are localized at one site k_j to form a composite particle (a cluster) at k_j . The wave function is given as

$$\Psi(1,2,\ldots,A) = \prod_{i=1}^{A} \phi_{k_j}(i).$$
 (C5)

This localized cluster wave function also has zero entanglement entropy, $S^{(1),i} = 0$. Let us next consider the following example of a strong correlation limit,

$$\Psi(1,2,\ldots,A) = \frac{1}{\sqrt{N_s}} \left\{ \prod_{i=1}^A \phi_{k_1}(i) + \prod_{i=1}^A \phi_{k_2}(i) + \cdots + \prod_{i=1}^A \phi_{k_{N_s}}(i) \right\},$$
(C6)

where A particles form a composite particle, and the composite particle moves freely in the whole space. This is a strongly correlated system, where, if a particle is observed at a certain site, all other particles are always observed at the same site. This is a strong coupling limit of the spatial correlation and corresponds to a delocalized cluster wave function of a cluster. I can easily get the one-body density operator

$$\hat{\rho}^{(1),i} = \sum_{j=1}^{N_s} \frac{1}{N_s} |k_j\rangle\langle k_j|,\tag{C7}$$

and the entanglement entropy $S^{(1),i} = \log N_s$.

Thus, the entanglement entropy indicates how a single particle is entangled with other particles. A localized composite particle has $S^{(1),i}=0$ because there is no entanglement even though particles have some spatial correlation in a sense. In contrast, if the delocalization of a composite particle occurs, $S^{(1),i}$ becomes finite and it is proportional to the logarithm of the number of sites (single-particle states) where the delocalization occurs. It indicates that the entanglement emerges because of the delocalization of the composite parcle.

Appendix D: Calculation of density matrix for linear $n\alpha$ states

In the present paper, I calculate matrix elements of the one-body density operator for linear-chain α -cluster states by the expansion of localized Gaussian bases,

$$\phi_{R_k}^{0s} = (\pi b^2)^{-3/4} \exp\left[-\frac{1}{2b^2}(\mathbf{r} - \mathbf{R}_k)^2\right],\tag{D1}$$

with $\mathbf{R}_k = (0, 0, R_k)$. For simplicity, I choose a species of nucleons, for instance, $p \uparrow$ and describe only the spatial part of $\sigma = p \uparrow$ nucleons because an $n\alpha$ -cluster state is spin-isospin symmetric. I take R_k with 0.75 fm intervals as $R_k = 0.75j$ fm $(j = 0, \pm 1, \ldots, 15)$, and prepare an orthonormal basis set $\{\phi_p(\mathbf{r})\}$ from the non-orthonormal Gaussian bases $\{\phi_{R_k}^{0s}(\mathbf{r})\}$ $(k = 1, \ldots, 35)$. For the bases $|p\rangle$, the one-body density matrix is written as

$$\rho_{pq} = \langle \Psi^{(A)} | c_q^{\dagger} c_p | \Psi^{(A)} \rangle,
= \int d\mathbf{r} d\mathbf{r}' \phi_p^*(\mathbf{r}) \rho^{(1)}(\mathbf{r}; \mathbf{r}') \phi_q(\mathbf{r}'), \tag{D2}$$

$$\phi_p(\mathbf{r}) = \langle \mathbf{r} | p \rangle.$$
 (D3)

By the diagonalization of ρ_{pq} , I can get the diagonalizing bases $|l\rangle$ by the unitary transformation of $|p\rangle$.

Appendix E: 3D-THSR wave functions of 2α

The deformed 3D-THSR wave function proposed by Funaki et al. [3] is given as

$$\Phi_{\text{3D-dTHSR}}^{2\alpha}(\beta_{\perp}, \beta_{z}) = \int d\mathbf{R}_{1} d\mathbf{R}_{2} \exp \left[-\sum_{i=1,2} \left\{ \frac{R_{ix}^{2} + R_{iy}^{2}}{\beta_{\perp}^{2}} - \frac{R_{1z}^{2}}{\beta_{z}^{2}} \right\} \right] \Phi_{\text{BB}}^{2\alpha}(\mathbf{R}_{1}, \mathbf{R}_{2}). \tag{E1}$$

The spherical 3D-THSR wave function of the case $\beta_{\perp} = \beta_z = \beta$ is written as

$$\Phi_{\text{3D-THSR}}^{2\alpha}(\beta) = \int d\mathbf{R}_1 d\mathbf{R}_2 \exp\left[-\sum_{i=1,2} \left\{\frac{\mathbf{R}_i^2}{\beta^2}\right\}\right] \Phi_{\text{BB}}^{2\alpha}(\mathbf{R}_1, \mathbf{R}_2). \tag{E2}$$

$$\propto \mathcal{A}\left[\prod_{i=1,2} \exp\left\{-\frac{\mathbf{X}_i^2}{\beta^2 + b^2/2}\right\} \phi(\alpha_i)\right],$$

$$\propto \mathcal{A}\left[\Phi_G(\beta) \exp\left\{-\frac{\mathbf{X}^2}{2\beta^2 + b^2}\right\} \phi(\alpha_1)\phi(\alpha_2)\right],$$

$$\Phi_G(\beta) \propto \exp\left\{-\frac{2\mathbf{X}_G^2}{\beta^2 + b^2/2}\right\} \tag{E3}$$

where $X_G = (X_1 + X_2)/2$ and $X = X_1 - X_2$, and $\Phi_G(\beta)$ is the c. m. motion. The wave function can be rewritten as

$$\Phi_{\text{3D-THSR}}^{2\alpha}(\beta) \propto \frac{\Phi_G(\beta)}{\Phi_G(0)} \int d\mathbf{R} \exp\left[-\frac{\mathbf{R}^2}{2\beta^2}\right] \Phi_{\text{BB}}^{2\alpha}(\mathbf{R}_1 = +\frac{\mathbf{R}}{2}, \mathbf{R}_2 = -\frac{\mathbf{R}}{2}). \tag{E4}$$

Appendix F: Extension to 3D system

The analysis with the entanglement entropy is applied to 1D cluster systems in the present paper. In principle, it is able to calculate entanglement entropy also in 3D systems. However, to extract information of correlations from the entanglement entropy of 3D systems, one may encounter a problem from trivial correlation due to the total angular momentum projection. Let us consider two particles (not identical to each other) in a spatial orbital with the angular momentum l. The L=0 state after the total angular momentum projection is given as $\sum_{\mu} \frac{1}{2l+1} |l,\mu\rangle \otimes |l,-\mu\rangle$ and it has the finite entanglement entropy $S=\log(2l+1)$. In the case that a cluster develops spatially, nucleons in a cluster have strong spatial correlations, which are generally characterized by the mixing of high l configurations, and therefore, S may reflect the many-body correlation in the cluster. However, one should take care that, even for a 0^+ state with a single j^2 configuration in the jj coupling shell model the entanglement entropy is finite as $S=\log(2j+1)$ because of the trivial correlation by the total angular momentum projection. It means that the entanglement entropy strongly depends on j of the major shell and such a large contribution from the angular momentum projection could make it difficult to extract information of pure correlations beyond the jj coupling configuration from the entanglement entropy.

^[1] Y. Fujiwara, Prog. Theor. Phys. Suppl. **68**, 29 (1980).

^[2] A. Tohsaki, H. Horiuchi, P. Schuck and G. Röpke, Phys. Rev. Lett. 87, 192501 (2001).

^[3] Y. Funaki, H. Horiuchi, A. Tohsaki, P. Schuck and G. Röpke, Prog. Theor. Phys. 108, 297 (2002).

^[4] Y. Funaki, A. Tohsaki, H. Horiuchi, P. Schuck and G. Ropke, Phys. Rev. C 67, 051306 (2003).

^[5] Y. Funaki, H. Horiuchi, W. von Oertzen, G. Röpke, P. Schuck, A. Tohsaki and T. Yamada, Phys. Rev. C 80, 064326 (2009).

^[6] B. Zhou, Z. Ren, C. Xu, Y. Funaki, T. Yamada, A. Tohsaki, H. Horiuchi and P. Schuck et al., Phys. Rev. C 86, 014301 (2012).

^[7] B. Zhou, Y. Funaki, H. Horiuchi, Z. Ren, G. Röpke, P. Schuck, A. Tohsaki and C. Xu et al., Phys. Rev. Lett. 110, 262501 (2013).

^[8] T. Suhara, Y. Funaki, B. Zhou, H. Horiuchi and A. Tohsaki, Phys. Rev. Lett. 112, 062501 (2014).

^[9] H. Morinaga, Phys. Rev. 101, 254 (1956).

^[10] Y. Suzuki, H. Horiuchi, and K. Ikeda, Prog. Theor. Phys. 47, 1517 (1972).

^[11] E. Uegaki, S. Okabe, Y. Abe and H. Tanaka, Prog. Theor. Phys. 57, 1262 (1977).

^[12] M. Chernykh, H. Feldmeier, T. Neff, P. von Neumann-Cosel and A. Richter, Phys. Rev. Lett. 98, 032501 (2007).

^[13] Y. Kanada-En'yo, Phys. Rev. Lett. 81, 5291 (1998).

^[14] Y. Kanada-En'yo, Prog. Theor. Phys. 117, 655 (2007) [Erratum-ibid. 121, 895 (2009)].

^[15] T. Suhara and Y. Kanada-En'vo, arXiv:1411.1240 [nucl-th].

^[16] E. Epelbaum, H. Krebs, T. A. Lahde, D. Lee and Ulf-G. Meissner, Phys. Rev. Lett. 109, 252501 (2012).

^[17] P. Chevallier, F. Scheibling, G. Goldring, I. Plesser and M. W. Sachs, Phys. Rev. 160, 827 (1967).

- [18] W. Bauhoff, H. Schultheis, and R. Schultheis, Phys. Rev. C 29, 1046 (1984).
- [19] N. Itagaki, A. Ohnishi, and K. Kato, Prog. Theor. Phys. 94, 1019 (1995).
- [20] S. Aberg, I. Ragnarsson, T. Bengtsson, and R. Sheline, Nucl. Phys. A391, 327 (1982).
- [21] M. Freer, M. P. Nicoli, S. M. Singer, C. A. Bremner, S. P. G. Chappell, W. D. M. Rae, I. Boztosun and B. R. Fulton et al., Phys. Rev. C 70, 064311 (2004).
- [22] T. Ichikawa, J. A. Maruhn, N. Itagaki and S. Ohkubo, Phys. Rev. Lett. 107, 112501 (2011).
- [23] D. M. Brink, International School of Physics "Enrico Fermi", XXXVI, p. 247, Academic Press, New York and London (1966).
- [24] Y. Kanada-En'yo, PTEP **2014**, 103D03 (2014).
- [25] C. H. Bennett, H. J. Bernstein, S. Popescu, and B. Schumacher, Phys. Rev. A 53, 2046 (1996).
- [26] P. Calabrese and J. L. Cardy, J. Stat. Mech. **0406**, P06002 (2004).
- [27] L. Amico, R. Fazio, A. Osterloh and V. Vedral, Rev. Mod. Phys. 80, 517 (2008).
- [28] T. Nishioka, S. Ryu and T. Takayanagi, J. Phys. A 42, 504008 (2009).
- [29] P. Ring and P. Schuck, gThe Nuclear Many-Body Problemh, Springer Verlag, New York (1980).